Modified Beta Algorithm for GMPPT and Partial Shading Detection in Photovoltaic Systems

Xingshuo Li, *Student Member, IEEE,* Huiqing Wen, *Member, IEEE,* Yihua Hu, *Senior Member, IEEE,* Lin Jiang, *Member, IEEE,* Weidong Xiao, *Senior Member, IEEE,*

***Abstract*—When the photovoltaic (PV) string is under the partial shading condition (PSC), the conventional Maximum power point tracking (MPPT) techniques may fail to track the global maximum power point (GMPP). Although some global MPPT (GMPPT) techniques have been proposed, they may overlook the GMPP and fail to detect the PSC occurrence. Therefore, a novel GMPPT technique is proposed in this paper by modifying the conventional Beta method. The proposed technique is more accurate than the previous techniques since it can guarantee that all the peaks in the β range and never overlook the GMPP. Furthermore, the proposed technique can inherently detect the PSC occurrence without setting any additional threshold parameters or periodical interruption, which is simpler and more effective. In order to verify the advantages of the proposed technique, a prototype with buck-boost converter was constructed. For a fair comparison, two popular GMPPT techniques were also implemented and tested in the same prototype under various scenarios. The performance improvement with the proposed technique for different partial shading conditions has been validated by both simulation and experimental results.**

***Index Terms*—Photovoltaic (PV) system, Global Maximum power point tracking (GMPPT), Beta algorithm, partial shading condition (PSC).**

I. Introduction

Maximum power point tracking (MPPT) technique are widely used in Photovoltaic (PV) systems since environmental conditions such as irradiance and temperature show strong effects on the actual output power of PV arrays. Many MPPT methods have been documented and compared [1, 2], such as Perturb and Observe (P&O) and Incremental Conductance (INC) method. These methods can successfully track the maximum power when uniform insolation is applied on the entire PV string since there is only one maximum power point (MPP). However, under the partial shading condition (PSC), due to the interference of clouds, trees or buildings, the actual output power of the PV system is significantly affected since these conventional MPPT methods are unable to differentiate the global MPP (GMPP) from the local MPPs (LMPP). Thus, conventional MPPT methods need to be modified in order to detect the PSC occurrence and improve the energy yield under any environmental condition.

To address the MPPT issues under PSCs, a number of global maximum power point tracking (GMPPT) methods have been discussed [5, 6]. According to the features of these GMPPT methods such as additional circuit requirements, tracking speed, and implementation complexity, this paper classifies these GMPPT techniques into three categories: soft computing (SC) methods, segmental search methods, and two-stage methods. The SC methods include fuzzy logic control

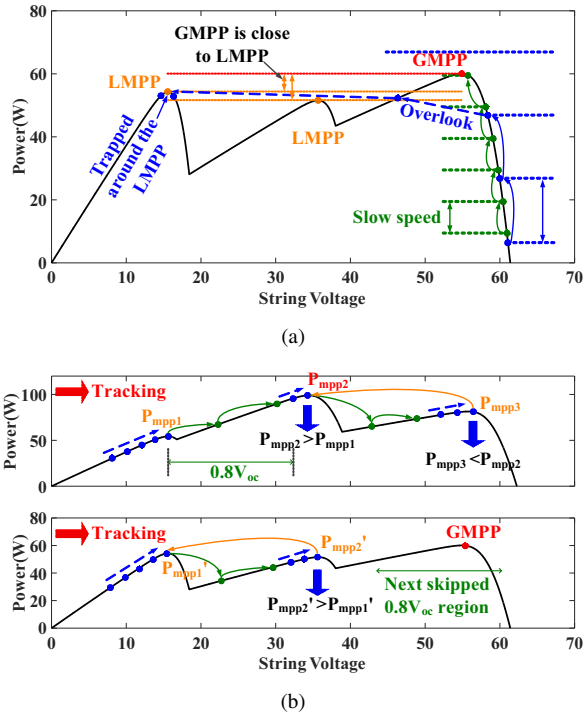

Fig. 1. Principle diagram of two advanced GMPPT techniques: (a)the technique in [3]; (b)the technique in [4].

(FLC) [7], particle swarm optimization (PSO) [8, 9], firefly algorithm (FA) [10], artificial bee colony (ABC) [11], Ant-colony optimization (ACO) [12], grey wolf optimization (GWO) [13] and simulated annealing (SA) [14], which shows good performance under different shading conditions. However, these intelligent methods are difficult in implementation such as the heavy calculation burden and the selection of initial point, which hinder the application in the commercial PV systems [6].

Segmental search methods are originated from the mathematical theories of dividing rectangle (DIRECT) technique [15], Fibonacci technique [16] and center point iteration technique [17]. The basic principle of these methods is to initially select an exploration range. Then, the exploration range is gradually reduced till finally locate the GMPP. These techniques are relatively simple and easy to implement. However, they may overlook the GMPP if an inaccurate segment is selected for further division.

The third category methods generally adopt two stages: in the first stage, an approximate GMPP location is determined

firstly from the LMPPs; then, in the second stage, the conventional MPPT techniques such as P&O and INC technique is used to locate the exact GMPP. Therefore, the key issue in designing these techniques is how to accurately determine the GMPP region in the first stage [6].

For this issue, various methods have been proposed and discussed. The load-line method was used in [18, 19] to allocate the operating point (OP) around the GMPP under the PSC. The advantage of the load-line method is its fast tracking speed. However, this method cannot guarantee that all GMPPs can be tracked [6].

The global-biased search method was proposed in [3]. This method employs a large interval to search the whole P-V curve in order to determine the largest peak value. The advantage of this method lies in its simplicity, while the disadvantage is also obvious since its performance highly depends on the selected global-biased search step [6]. A too large step may overlook the GMPP, while a too small step requires more tracking time, as shown in Fig. 1(a). Furthermore, when the value at the GMPP is close to those at these LMPPs, this method is easy to be trapped at the LMPPs, especially by using a large step [6].

The method discussed in [4, 20–22] is named as the "$0.8V_{oc}$ model method", which is originated from the prior assumption that the peaks of a P-V curve under the PSC occur nearly at multiples of 80% of V_{oc}. Compared to the global-biased search method, the $0.8V_{oc}$ model method only searches the vicinity of the $0.8V_{oc}$ regions rather than the entire P-V curve. Thus, this $0.8V_{oc}$ model method is more effective than other two-stage methods. However, taking the technique in [4] as an example, there are several drawbacks for this $0.8V_{oc}$ model method. Firstly, the overall tracking speed is generally slow since each peak must be determined by the incremental conductance (INC) method, marked as blue points in Fig. 1(b). Secondly, technique in [4] may overlook the GMPP. As shown in Fig. 1(b), once a new peak is tracked, this peak will be compared with the previous peak. If this peak is larger than the previous one, such as $P_{mpp2} > P_{mpp1}$, the operating point will move towards the next $0.8V_{oc}$ region. Once the new peak is smaller than the previous one, such as $P_{mpp3} < P_{mpp2}$, the algorithm will skip the next $0.8V_{oc}$ region, return to the previous peak and stop the tracking process. However, if the real GMPP happens to be at the next skipped $0.8V_{oc}$ region, the algorithm will be trapped at the LMPP and the overall efficiency will be reduced. Furthermore, even if the real GMPP is not skipped, [23] pointed out that $0.8V_{oc}$ model is not always true, especially for long PV strings. It may scan the wrong region of the P-V curve and lead to incorrect global peak detection.

How to detect the PSC occurrence is also an important performance index for GMPPT techniques. The aforementioned methods generally set a threshold for power change [20, 22] or voltage and current change [4, 15, 17, 19, 21]. However, under some conditions, due to the change of shading patterns, the detection result of the PSC occurrence may be incorrect [6]. Thus, some GMPPT techniques are proposed by setting a timer in the algorithms to periodically execute these techniques [3, 4, 20]. However, if there is no changes in the solar irradiance or shading pattern, unnecessary energy loss is generated due to the periodical interruption.

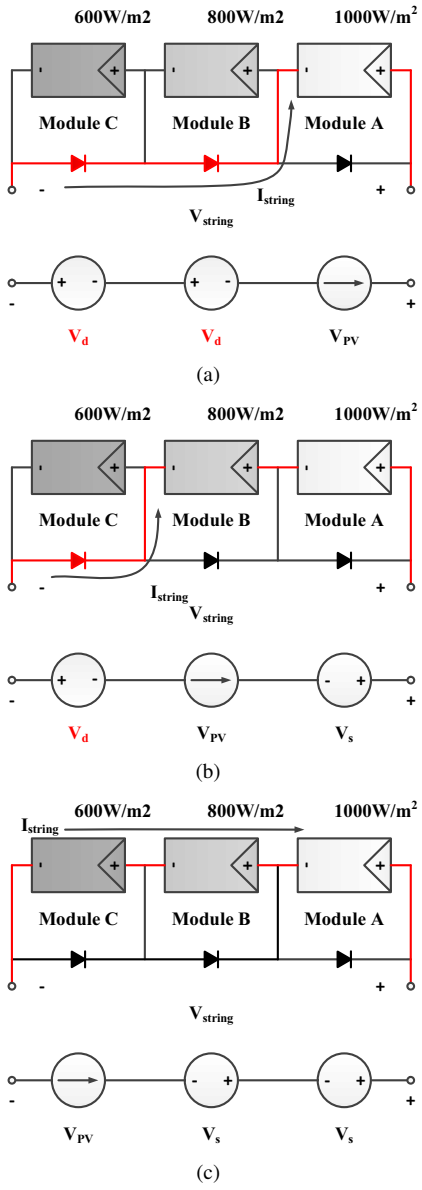

Fig. 2. Operation stages of a PV string under partial shading. (a) Stage I: two bypass diodes conducted. (b) Stage II: one bypass diode conducted. (c) Stage III: no bypass diode conducted.

In this paper, by modifying the conventional Beta method [24–26], a novel two-stage GMPPT method is proposed to predict the position of GMPPT for PV arrays under PSC. Firstly an equivalent PV string model is obtained for various shading patterns. An explicit expression of the string voltage with the string current is derived. The proposed method searches the vicinity of the parameter β rather than $0.8V_{oc}$, which overcomes the defects of the the "$0.8V_{oc}$ model methods", scan the wrong region of the P-V curve and incorrect global peak detection. In detecting the PSC occurrence, no threshold parameters or periodical interruption is required and the implementation difficulty is reduced. Both simulation and experimental results on a PV string under various shading conditions are presented to verify the advantages of the proposed

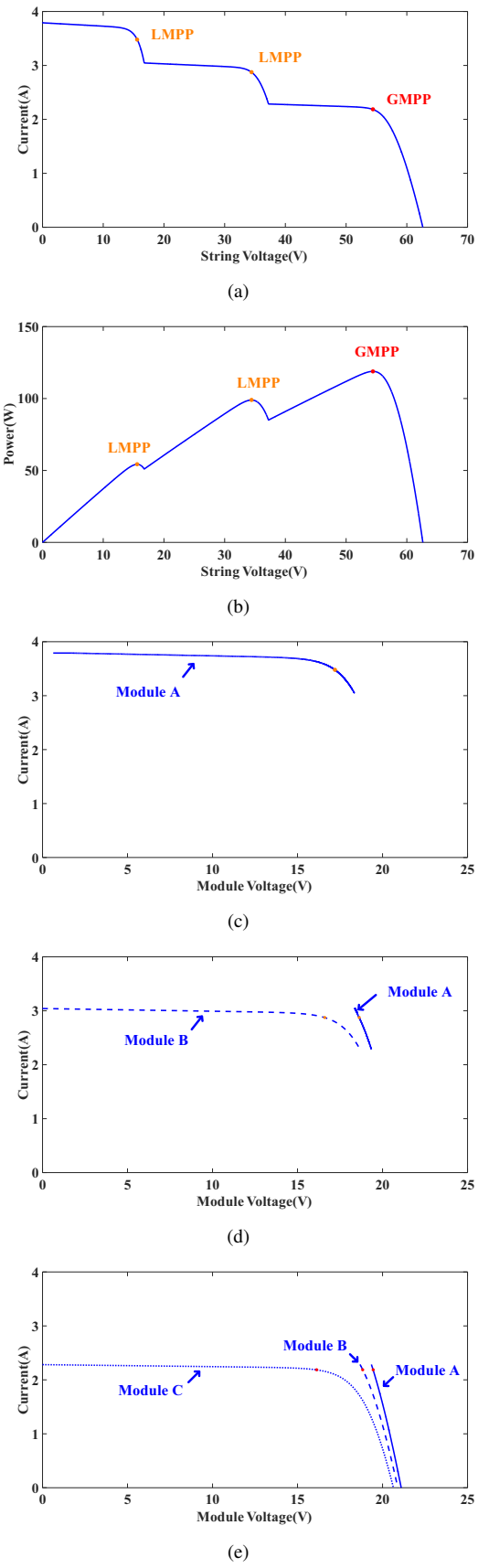

Fig. 3. (a) I–V curve of the PV string; (b) P–V curve of the PV string; (c) Detailed I–V curve of each module for stage I;(d) Detailed I–V curve of each module for stage II; (e) Detailed I–V curve of each module for stage III.

method.

II. PV STRING EQUIVALENT MODEL

A. Operation Stages and Key Module

Fig. 2 shows the operation stages of a PV string and the equivalent circuits under partial shading conditions. In this PV string, three modules are connected in series with different solar irradiance. More specifically, only module A is fully illuminated with 1000 W/m^2, while module B and module C are partial shaded, whose irradiances are reduced to 800 W/m^2 and 600 W/m^2. Each module has a bypass diode in parallel to avoid the occurrence of hot spot under the PSC [23]. According to the string current variation, the operation of the PV string can be categorized into three different operation stages and each stage presents one peak. Fig. 3(a) and (b) illustrate the corresponding I–V curve and P–V curve of the PV string, three peaks are observed and labeled in both I–V curve and P–V curve, namely two LMPPs and one GMPP. In order to clearly illustrate the operation of each module in this PV string, Fig. 3(c) to (e) illustrate the individual I–V curves of these three modules for different operation stages. For each stage, one key module can be specified, which is dominated to determine the string current. For other modules, there are two possibilities. One is independent voltage source V_d due to the corresponding conducted bypass diode, while the other is linear voltage source V_s if the irradiation of this module is higher than that of the key module. The detailed analysis for each operation stage is described in the following paragraphs.

Stage I: in this stage, two shaded modules, namely module B and module C, are bypassed by the diodes. As illustrated in Fig. 3(c), this stage shows the highest string current and the lowest string voltage. The string current is determined by the characteristic of module A since it is exerted by the highest illumination. At the meantime, the modules B and C show characteristics of independent voltage sources V_d, corresponding to the forward voltage drop of the bypass diodes [27], as highlighted with the red color in Fig. 2(a). During this stage, one LMPP is observed and illustrated both in Fig. 3(a) and (b).

Stage II:in this stage, due to the reduction of the string current, only one module (namely module C) is bypassed and module B becomes the key module. Thus, module C can be simply represented as V_d. At this time, module A works as a linear voltage source V_s [27] since the sun intensity for module A is higher than that of key module B. The characteristic of module A is determined by the relationship of the string current and the module short-circuit. Fig. 2(d) illustrates the individual I–V curves for both module B and module A: classical I–V curve presented for module B under irradiation of 800 W/m^2 , however, the I–V curve for module A is approximated as a straight line. During this stage, one LMPP is observed, as illustrated both in Fig. 3(a) and (b).

Stage III: due to further reduction of the string current, no module is bypassed and module C becomes the key module, where it has the lowest sun intensity. Both module A and B operate as linear voltage sources since the sun intensities for these two modules are higher than that of key module C.

Fig. 2(e) illustrates the I–V curves for these modules: classical I–V curve presented for module C under irradiation of 600 W/m^2 , however, the I–V curves for both module A and B are approximated as straight lines.

B. PV String Equivalent Model

From Fig. 3, it can be seen that the I–V curve of the PV string is always determined by the key module since the other modules are approximately constant or linear [27]. Originated from this phenomenon, it's possible that the GMPP tracking process for one long PV string can be simplified as MPP tracking process for the key modules of the PV string during different operation stages.

The equivalent voltage of the key module V_{eq} can be expressed by

$$V_{eq} = V_{String} - (n-1) \times V_s + (m-n) \times V_d \tag{1}$$

where V_{String} represents the output voltage of the PV string, m refers to the total number of PV modules in the PV string, and n is determined by

$$n = \begin{cases} 1, & \text{for } 0 < V_{String} <= \alpha \cdot V_{oc} \\ 2, & \text{for } \alpha \cdot V_{oc} < V_{String} <= 2 \cdot \alpha \cdot V_{oc} \\ \ldots & \\ m, & \text{for } (m-1) \cdot \alpha \cdot V_{oc} < V_{String} <= m \cdot \alpha \cdot V_{oc} \end{cases} \tag{2}$$

where V_{oc} is the open-circuit voltage of PV modules, α is a variable that is varying from 0.8 to 0.97 [23]. According to [23], $\alpha = 0.95$ can cover In this paper, α is set as 0.95, which can guarantee all peaks located in their own divided segments.

In (1), V_d is forward voltage drop of the diodes, which is usually set as $0.8V$. V_s is a linear voltage source, which can be approximately expressed by [27, 28]

$$V_s \approx \frac{V_{MPP,stc} - V_{oc,stc}}{I_{MPP,stc}} \times I_{String} + V_{oc,stc} \tag{3}$$

where $V_{MPP,stc}$ and $I_{MPP,stc}$ represent voltage and current at the MPP under the standard test condition (STC), I_{String} refers to the current of the PV string.

III. Proposed Algorithm

A. Modifed Beta Method

With the explicit PV string model, a complicated global maximum power point (GMPP) procedure for a PV string under PSC can be significantly simplified by directly tracking for each MPP of key module for different operation stages individually. Among various MPPT algorithm for PV systems, the Beta method proposed by Jain and Agarwal shows significant advantages such as fast tracking speed, zero oscillations for steady state, and simple implementation [2]. In this paper, the conventional Beta method is modified in order to predict the position of global maximum power point (GMPP) during partial shading. The basic principle of this method is to track an intermediate variable β rather than the change of the power, which is expressed as [24–26]:

$$\beta = ln\left(\frac{i_{pv}}{v_{pv}}\right) - c \times v_{pv} \tag{4}$$

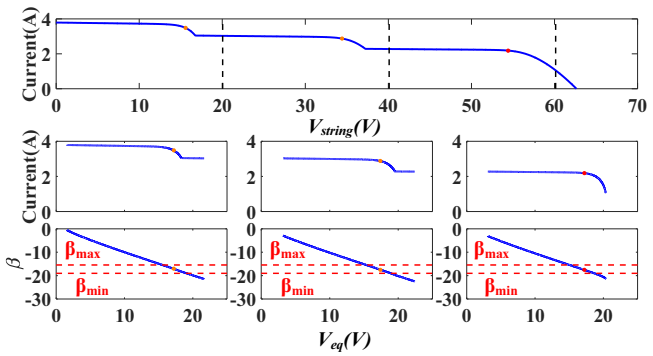

Fig. 4. I–V curve for the PV String and the corresponding curves of V_{eq} and β_{eq} for different stages.

where v_{pv} and i_{pv} are the PV module output voltage and output current respectively. $c = q/(N_s AKT)$ is the diode constant, where q is the electron charge $1.602 \times 10^{-19} C$, A is the diode ideality factor, K is Boltzmann constant $1.38 \times 10^{-23} J/K$, T(in Kelvin) is the temperature of the p–n junction, and N_s is cell number of the PV module.

With the equivalent PV string model shown in Fig. 2, the equivalent value of β, β_{eq}, can be determined by the following expression:

$$\beta_{eq} = ln\left(\frac{I_{String}}{V_{eq}}\right) - c \times V_{eq} \tag{5}$$

Fig. 4 illustrates I–V curve for the PV String and the corresponding curves of V_{eq} and β_{eq} for different stages. In the top of Fig. 4, the I–V curve of the PV string is divided into four segments. Since the power peaks unlikely occurs in the rightmost segment of the I–V curve, the left three segments are considered. The equivalent I–V curves for key modules during these segments are illustrated in the middle of Fig. 4. Then, the equivalent β–V curves are obtained by (4) and illustrated in the bottom of Fig. 4. From the equivalent β–V curves, it can be seen that all the peaks are located in the defined range of β. The bounding range of (β_{min}, β_{max}) depends on the environmental conditions of the PV module, such as the irradiance and temperature. An explicit expression for β_{min} and β_{max} is presented in [29]. Furthermore, the changes of β_{eq} can be also used to detect whether the PSC occurs.

B. Algorithm Flowchart and Tracking Process

The flowcharts of the proposed technique is shown in Fig. 5. As shown in Fig. 5(a), the proposed technique initially senses I_{String} and V_{String}, and V_{eq}, n, V_s and β_{eq} are determined by (1)-(5). Then, the main algorithm loop of the proposed technique is divided into three branches, namely Adaptive Scaling Factor Beta method (ASF-Beta), Zero Oscillations Perturb and Observe (ZO-PO) and Search Mode, as illustrated in Fig. 5. Different colors are used in order to distinguish these branches. In the main loop, basically there are two criterion adopted for the algorithm implementation. The first criteria is to detect if the calculated β_{eq} is located within the defined range. Then, a variable "Flag" is used to determine the

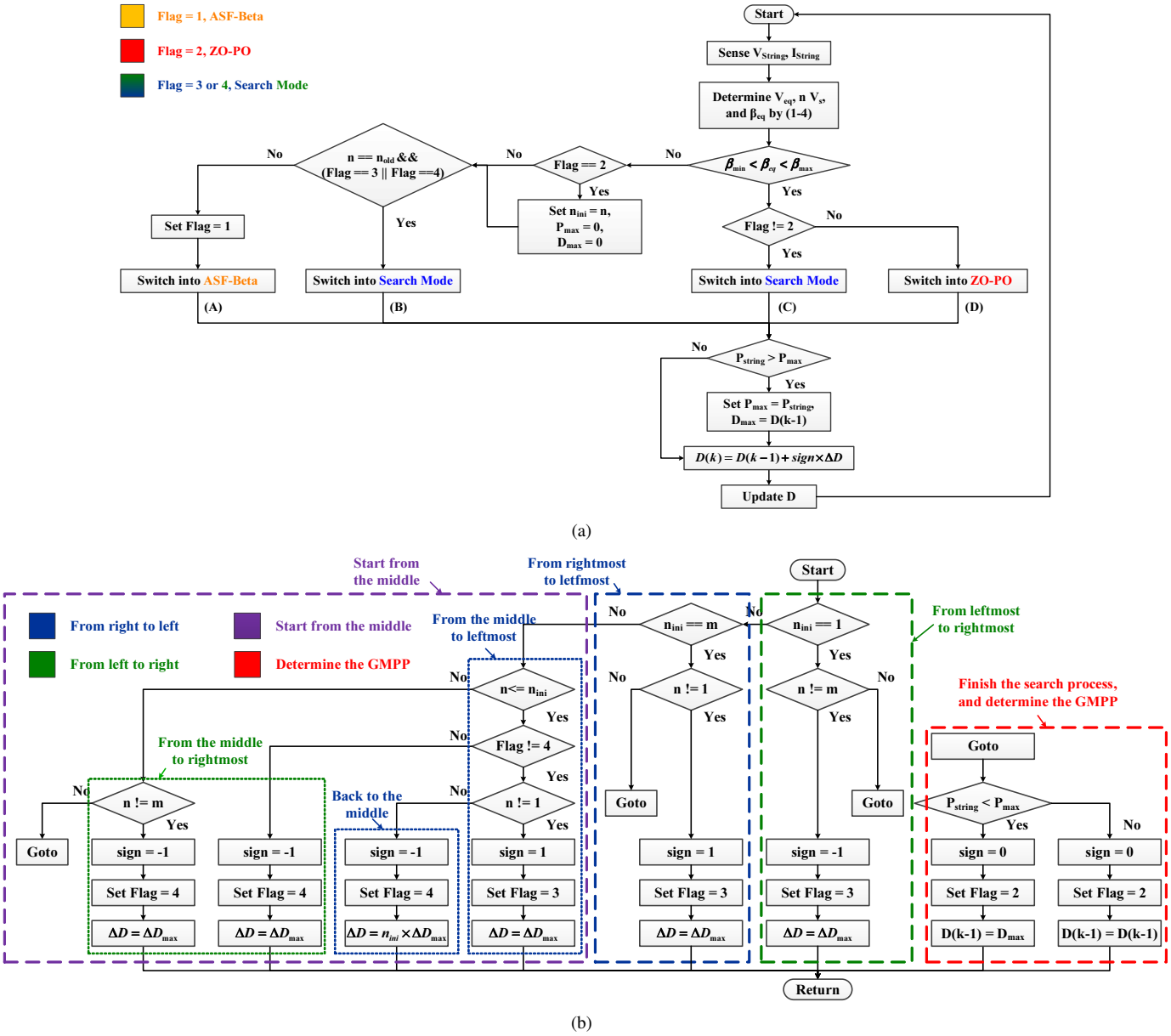

Fig. 5. Flowchart of the proposed method: (a) Main Loop. (b) Search mode.

algorithm branch. The ASF-Beta branch is used to fast locate the OP within the range of β [29, 30]. Once the ASF-Beta reaches the β range, the Search Mode branch is triggered, as illustrated in as shown in Fig. 5(b). According to the position of OP, the OP may move from the right to left, from the left to right, or from the middle, which illustrated with different colors in 5(b). In 5(b), another branch is used to determine the GMPP and finish the Search Mode branch. Repeating this process, the ASF-Beta locates the next β range and the Search Mode is triggered again until all of the β range are tracked. Finally, the vicinity of the GMPP is determined and the ZO-PO branch is triggered in order to track exactly the location of GMPP.

In order to help understand the principle of the proposed technique, detailed tracking process for a PV string with three modules under both the uniform condition and PSC conditions is given in Fig. 6, where Fig. 6 (a) and (b) shows the typical curves under the uniform condition while Fig. 6 (c) and (d) illustrates the typical curves under the PSC.

Initially, the PV system starts up under the uniform irradiance, where the solar irradiance under all of the PV modules is $1000W/m^2$. Thus, the tracking process under the uniform condition is shown as below:

In step (1), the GMPPT of the PV system is assumed to start up from the rightmost, as shown in Fig. 6(a). The initial value of n, namely n_{ini}, is set as 3, which is the total number of PV modules in this string. In step (2), since the value of β_{eq} is calculated out of the range of β, "Flag" is set as 1. As a consequence, the proposed technique goes through the branch (A), as shown in Fig. 5(a). The ASF-Beta method is triggered to gradually reach the β range in the "region $n = 3$". At time $0.18s$, the ASF-Beta method locates the first β range. Then,

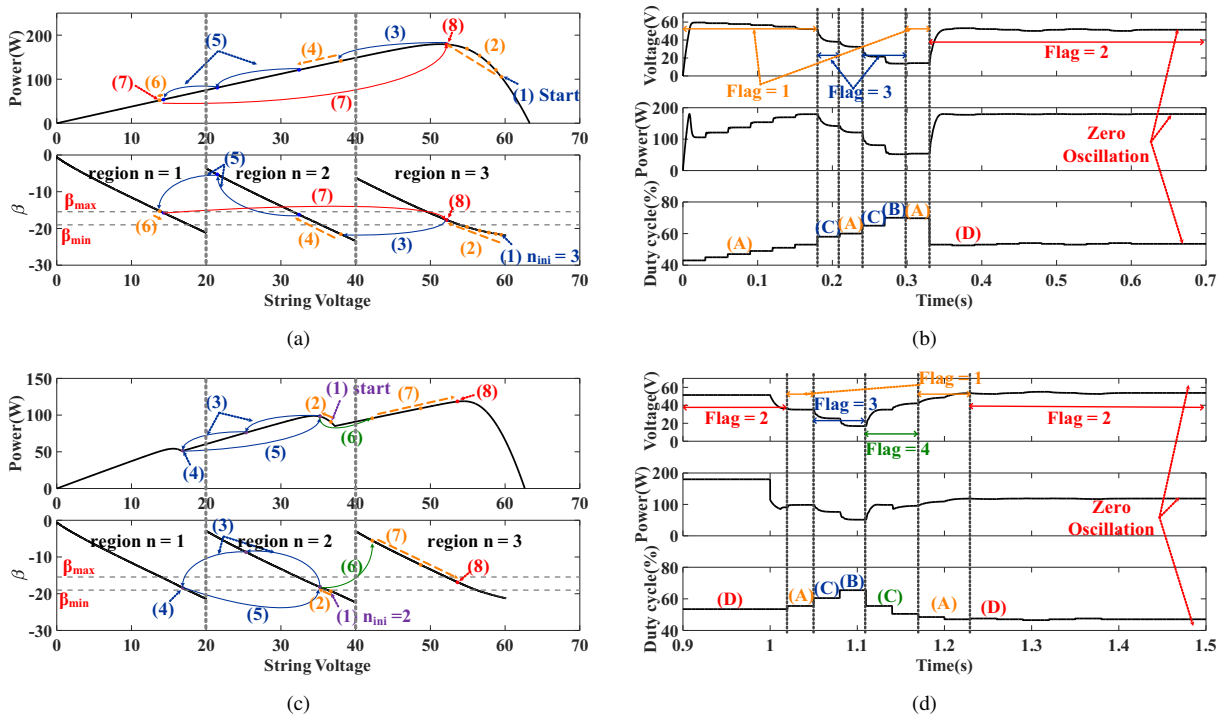

Fig. 6. Tracking process of the proposed technique. (a) Typical curves with respect to the string voltage under the uniform condition. (b) Typical curves with respect to time under the uniform condition. (c) Typical curves with respect to the string voltage under the PSC. (d) Typical curves with respect to time under the PSC.

in step (3), the proposed technique goes through the branch (C) in Fig. 5(a) to trigger the Search Mode. Since there are three modules in this PV string, m is equal to 3. Therefore, the condition "$n_{ini} == m$" is satisfied, marked as blue block in Fig. 5(b). Then, "sign" is set as 1 and "Flag" is set as 3, which means OP moves towards the left. At time $0.21s$ in step (4), the OP reaches the "region $n = 2$" from the "region $n = 3$". Then at time $0.24s$, the ASF-Beta method is triggered again and reaches the next β range. Then, in step (5), the proposed technique goes through the branch (C), and the Search Mode is triggered again to move towards the left. However, at the time $0.27s$, the OP is still in the previous "region $n = 2$". Therefore, the condition "$n = n_{old}\&\&(Flag == 3||Flag == 4)$" is satisfied, as shown in Fig. 5(a). As a consequence, the proposed technique goes through the branch (B) to force the OP moving towards the left until reaching the "region $n = 1$". At time $0.3s$, the OP reaches the region "$n = 1$". Then, in step (6), the ASF-Beta method is triggered again. At time $0.33s$, the OP reaches the β range in the "region $n = 1$". In step (7), since the condition "$n! = 1$" is not satisfied, the Search Mode detect that all of the β range has been searched. Then, the proposed technique goes into the determination process, which is marked as red block in Fig. 5(b). As a consequence, the proposed technique finds out that the area of the GMPP is in the "region $n = 3$", and the OP goes back to the "region $n = 3$". After that, the proposed technique goes into the branch (D), and the ZO-PO method is triggered to find the exact location of the GMPP. After several steps, in step (8), the exact location of the GMPP is found, furthermore, there is no steady-state oscillation at the GMPP.

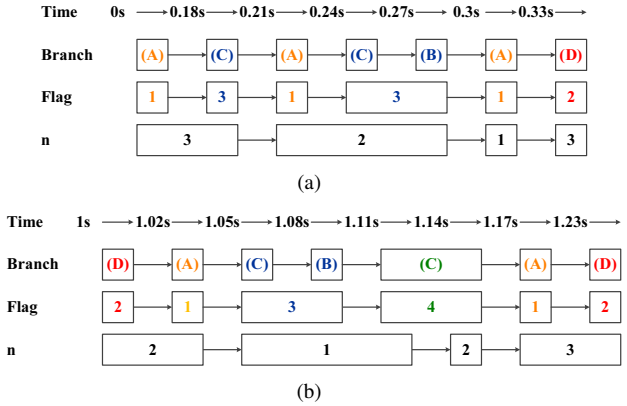

Fig. 7. Variations of the branch loop and variables during the whole tracking process by using the proposed technique. (a) Under the uniform condition. (b) Under the PSC.

Then, at time $1s$, two modules are shaded and the irradiance decreases to $800W/m^2$ and $600W/m^2$ respectively, as shown in Fig. 6(c) and (d). Thus, the tracking process is switched from the uniform condition to the partial shading condition and the detailed process is described as below:

At time $1s$ in step (1), the partial shading happens as shown in Fig. 6(d). Then, at time $1.02s$, the proposed technique detects the value of β_{eq} is out of the range of β. Hence, the PSC is detected by this. At this moment, the OP is located in the "region $n = 2$". Thus, n_{ini} is set as 2, and P_{max} and D_{max} are cleared. Then, in step (2), the proposed technique goes through the branch (A). "Flag" is set as 1, and the ASF-Beta method is triggered. At time $1.05s$, the first β range in

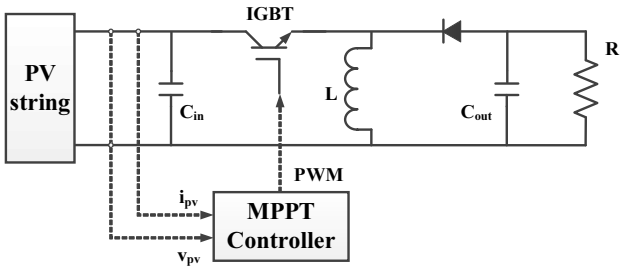

Fig. 8. Diagram of the PV system.

the "region $n = 2$" is located. In step (3), since n_{ini} is equal to 2, both of the condition "$n_{ini} == m$" and "$n_{ini} == 1$" are not satisfied. The Search Mode goes through the purple block, as shown in Fig. 5(b). Then, the proposed technique uses two steps to reach the "region $n = 1$" at time $1.11s$. At time $1.11s$ in step (4), the OP is detected already in the β range in the "region $n = 1$". Therefore, the proposed technique skips the ASF-Beta method and directly triggers the Search Mode again. At the meanwhile, in step (5), the proposed technique identifies that the OP is in the leftmost. In order to distinguish that the leftmost has been already reached, the "Flag" is set as 4, as shown in Fig. 5(b). Thus, the OP comes back to the middle in the "region $n = 2$" at time $1.14s$., and move towards the right. Then, in step (6), the OP moves to the "region $n = 3$" at time $1.17s$ by triggering the the Search Mode. In step (7), The ASF-Beta method is triggered again, and locates the β range at time $1.23s$. Finally, in step (8), all of the β range has been searched, and the proposed technique finds out that the current OP is in the area of the GMPP. Therefore, the ZO-PO method is triggered to find the exact location of the GMPP.

Finally, Fig. 7 summarises the detailed variations of the branch loop and variables during the whole tracking process for the proposed technique for both the uniform condition and PSC.

IV. Simulation Evaluation

A. Simulation Setup

Fig.8 shows the diagram of the PV system, which includes a PV string, buck-boost converter, resistive load and MPPT controller. The Solarex MSX-60W is used and main electrical parameters are shown in TABLE I. Main specifications for the buck-boost converter include: C_{in} = $470uF$, C_{out} = $47uF$, L = $1mH$, switching frequency (IGBT) = $20kHz$, resistive load = 20Ω. The sampling time for the MPPT controller, T_p, is set as $0.03s$.

In order to evaluate the effectiveness of the proposed MPPT technique, simulation comparison of the proposed MPPT technique with other GMPPT techniques is conducted in Matlab/Simulink 2015a. For a fair comparison, two typical two-stage GMPPT techniques are selected, namely the technique in [3] and the technique in [4]. Since the performance of the technique in [3] highly depends on the selected global-biased search step, $\Delta P_{interval}$, two different values of $\Delta P_{interval}$, specifically $20W$ and $10W$, are used. Furthermore, considering that both the technique in [3] and the technique in [4] adopt the P&O or INC technique in the second stage, which is the same as the proposed method, thus, in this comparison, a fixed step size for these methods is set as 0.5%.

TABLE I
Main Product Parameters of the MSX-60W

Parameter	Symbol	Value
Maximum power	P_{mpp}	$60W$
Voltage at maximum power	V_{mpp}	$17.1V$
Current at maximum power	I_{mpp}	$3.5A$
Open-circuit voltage	V_{oc}	$21.1V$
Short-circuit current	I_{sc}	$3.8A$
Temperature coefficient of V_{oc}	K_v	$-80mV/°C$
Temperature coefficient of I_{sc}	K_i	$0.065\%/°C$

In this simulation, there are three PV modules connected in series in the PV string (donated as 3s1p), which is commonly used for the GMPPT investigation, such as [22]. For the 3s1p PV string with three peaks, there are six PSC patterns for the characteristics of P–V curves, as shown in Fig.9. For Pattern I and Pattern IV, the highest peak (refers as 1) is in the right or the left respectively, while the highest peak for Pattern II and Pattern V is in the middle. For Pattern III and Pattern VI, the highest peak is also in the right or the left, however, their lowest peak (refers as 3) is in the middle. From Fig.9, it can be seen that the trends of Pattern I, Pattern II and Pattern III are opposite to the trends of Pattern IV, Pattern V and Pattern VI. Therefore, only Pattern I to Pattern III are considered in this simulation, as illustrated in Fig.10.

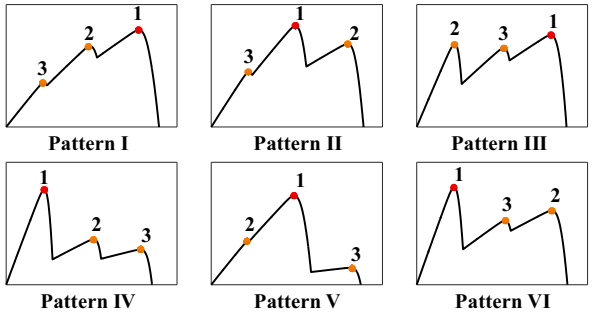

Fig. 9. Different PSC patterns for 3s1p PV string.

B. Simulation Results

Fig.11 to Fig.13 illustrate the simulation results for Pattern I to Pattern III with the numerical results. As shown in Fig.11 (a) and (b), the technique in [3] initially starts from the vicinity of the string open-circuit voltage, and then the rest of the P–V curve is scanned by using $\Delta P_{interval}$. Fig.11(a) shows that the technique in [3] with a small $\Delta P_{interval}$ requires 15 steps to finish the scanning and detect the vicinity of GMPP at time $0.45s$. The same technique with a large $\Delta P_{interval}$ only needs 8 steps to detect the area of the GMPP. However, it requires 6 more steps to finally locate the real GMPP by using the P&O method.

The technique in [4] initially find the first MPP by using the INC method, as shown in Fig.11(c). Then, this technique

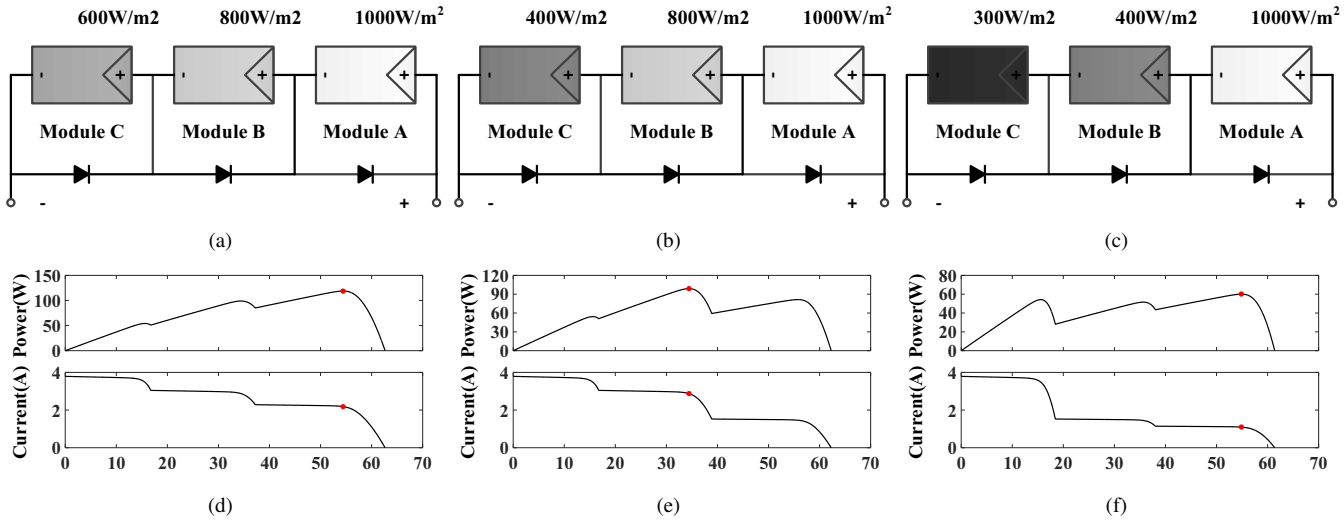

Fig. 10. Different PSC patterns: (a)Pattern I; (b) Pattern II; (c) Pattern III; (d) Curves for pattern I; (e) Curves for pattern II; (f) Curves for pattern III.

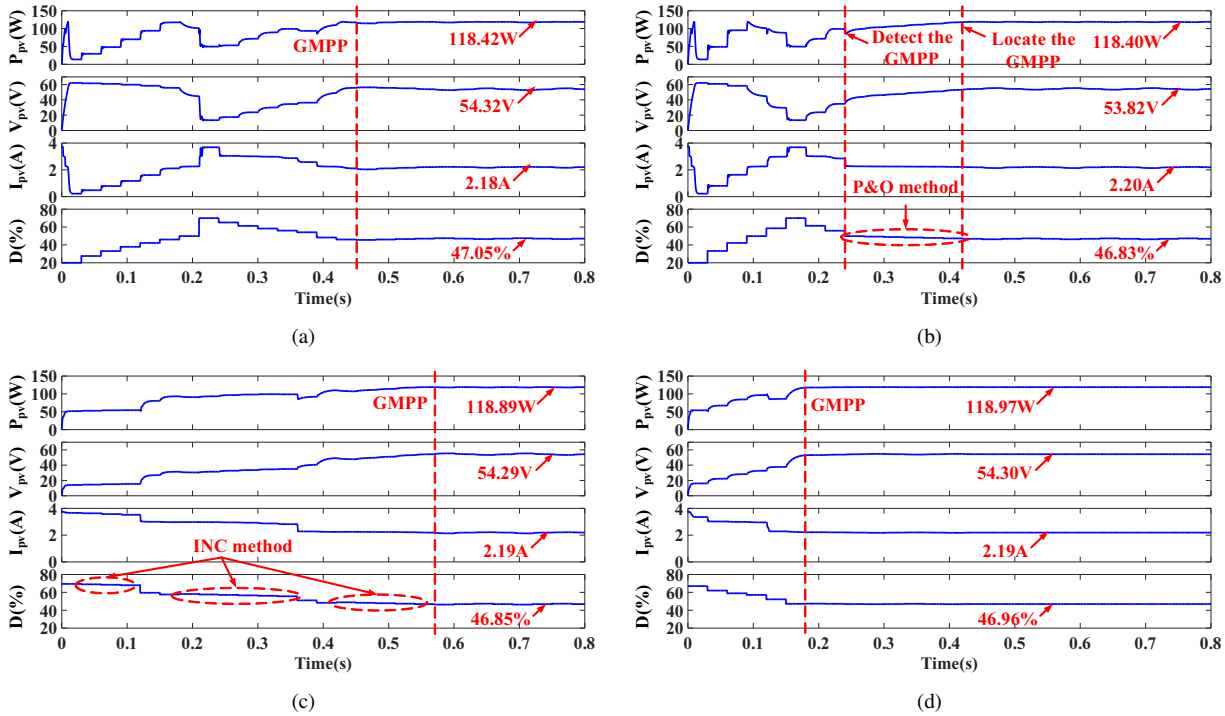

Fig. 11. Simulation results for pattern I: (a) the technique in [3] with $\Delta P_{interval} = 10W$; (b) the technique in [3] with $\Delta P_{interval} = 20W$; (c) the technique in [4]; (d) the proposed technique.

directly jumps to the vicinity of the second MPP with the $0.8V_{oc}$ voltage increment and gradually find the second MPP by using the INC method. This process is repeated until the power at the next MPP is smaller than the previous one, or the operating point reaches the rightmost of the P–V curve. Since each MPP must be determined by the INC method, this technique requires the longest time to locate the GMPP, specifically $0.57s$ as indicated in the simulation.

Compared to the technique in [4], the proposed technique just reaches the vicinities of the each MPPs rather than the exact locations. Thus, the proposed technique requires less time to locate the GMPP. The global searching by using the proposed technique targets the GMPP directly since these vicinities are easily located within the β ranges. As shown in Fig.11(d), for the Pattern I, the proposed technique requires the least time to locate the GMPP, which is only 6 steps. Furthermore, the proposed technique shows higher accuracy than the technique in [3] and shows zero oscillation for the steady state.

Fig.12 shows the simulation results for the pattern II. It shows that the proposed one is fastest to locate the GMPP, which only requires $0.27s$, while the technique in [3] with $\Delta P_{interval} = 20W$ and $\Delta P_{interval} = 10W$ requires $0.3s$ and $0.42s$, respectively. In the comparison, the technique in [4]

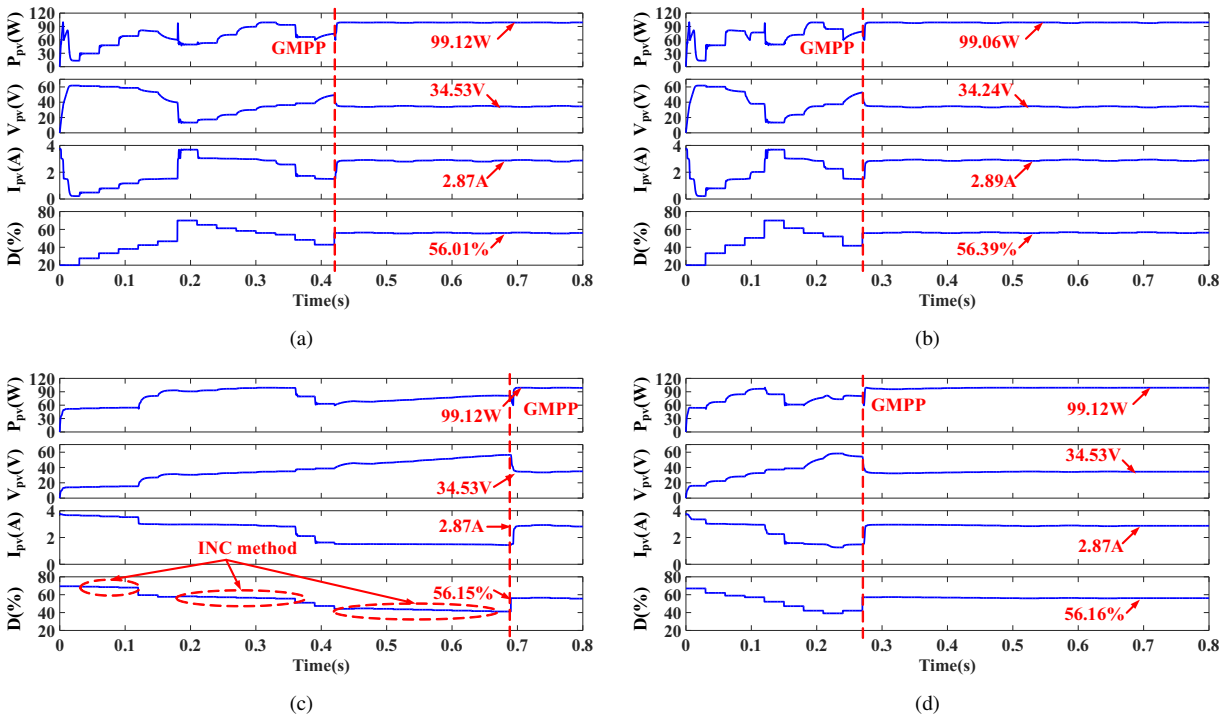

Fig. 12. Simulation results for pattern II: (a) the technique in [3] with $\Delta P_{interval} = 10W$; (b) the technique in [3] with $\Delta P_{interval} = 20W$; (c) the technique in [4]; (d) the proposed technique.

requires the longest time to locate the GMPP, which is $0.69s$.

Fig.13 shows the simulation results for the pattern III. It shows that only the proposed technique and the technique in [3] with $\Delta P_{interval} = 10W$ can correctly locate the GMPP, which requires $0.3s$ and $0.48s$ respectively. The technique in [3] with $\Delta P_{interval} = 20W$ and the technique in [4] can only track the LMPPs. In order to clearly explain the reason for the tracking failure, some details for Pattern III are illustrated in Fig.14.

Fig.14(a) and (b) shows the tracking processes of the technique in [3]. Initially, this technique starts from the vicinity of the string open-circuit voltage and search the P–V curve by $\Delta P_{interval}$, which is marked as the dash lines in Fig.14(a) and (b). In Fig.14(a), the successive movement of the OPs is followed as the trajectory $P_1 \rightarrow \cdots \rightarrow P_5$ by $\Delta P_{interval} = 10W$. At point P_5, the reduction of the power is found and point P_4 is identified as the highest point among P_1 to P_5, Then, the OP moves to point P_6, and the successive movement of the OPs is followed as the trajectory $P_6 \rightarrow \cdots \rightarrow P_{14}$ by $\Delta P_{interval} = 10W$. At point P_{14}, the whole P–V curve has been scanned and the point P_4 is still the highest one. Therefore, the OP directly moves to point P_4, the P&O method is executed in order to exactly locate the GMPP, and finally point P_{15} is located.

In Fig.14(b), the OPs successively moves by $\Delta P_{interval} = 20W$. At point P_2, according to the parameter of $\Delta P_{interval} = 20W$, the next OP should be point P_3'. However, since the increment of power line is too large, point P_3' is not located within the P–V curve. Therefore, the OP moves to point P_3, which overlooks the first MPP. Similarity, the next supposed OP P_4' is also not located at the P–V curve, the actual OP moves to point P_4, which overlooks the second MPP again. At point P_6, the whole P–V curve has been scanned and the point P_5 is regarded as the highest one. Then, the P&O method is executed and P_7 is mistakenly founded as the GMPP.

Fig.14(c) shows the tracking process of the technique in [4]. Initially, this technique starts with the INC method, which is marked as blue dash arrow with (1). When the first MPP is located by the INC method, this technique goes into its subroutine, which is marked as green curve arrows with (2). In its subroutine, the reference voltage V_{ref} is determined by

$$V_{ref} = V_{mpp1} + 0.8 \times V_{oc} \tag{6}$$

where V_{mpp1} is the voltage at the first MPP. Then, the next duty cycle $D(k)$ is determined by

$$D(k) = \frac{\sqrt{R_{load}}}{\sqrt{R_{load}} + \sqrt{R_{pv}}} \tag{7}$$

where R_{load} refers to the resistive load, which is equal to 20Ω, and R_{pv} is determined by

$$R_{pv} = \frac{V_{ref}}{I_{string}(k-1)} \tag{8}$$

The process of this subroutine is repeated until the different in current ΔI is smaller than a threshold ΔI_{min}, which is set as $0.2A$ in this paper. Then, the INC method is executed again and the second MPP is found, which is marked as blue dash arrow with (3). Since the value of P_{mpp2} is smaller than that of P_{mpp1}, this technique returns the first MPP, which is marked as yellow curve arrow with (4), and mistakenly believed that point P_{mpp1} is the GMPP.

In Fig.14(d), the tracking process of the proposed technique is illustrated. Initially, this technique starts with the ASF-Beta

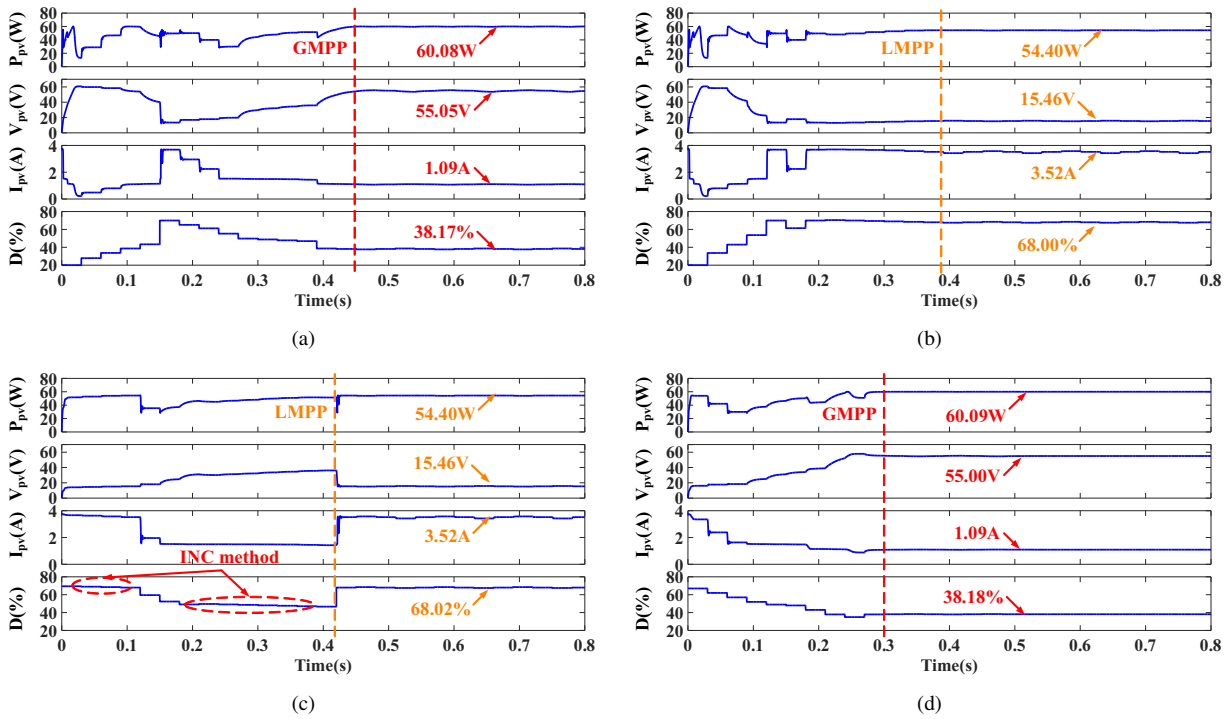

Fig. 13. Simulation results for pattern III: (a) the technique in [3] with $\Delta P_{interval} = 10W$; (b) the technique in [3] with $\Delta P_{interval} = 20W$; (c) the technique in [4]; (d) the proposed technique.

method, which is marked as yellow dash arrow with (1). When the OP reaches the first β range, the Search Mode starts and skips to the vicinity of the "region $n = 2$", which is marked as green curve arrows with (2). Then, the ASF-Beta method and the Search Mode are alternatively triggered as the trajectory (3) $\rightarrow$ (4) $\rightarrow$ (5). After (5), all of the β ranges are scanned, and the GMPP is identified in the "region $n = 3$". Then, the ZO-PO method is triggered to locate the real GMPP and reduce the oscillation in the steady state.

C. Load Variation

Fig.15 illustrates the simulation results for the load variation condition. Initially, the load resistance R_{load} is set as 20Ω. At time $0.5s$, R_{load} is changed to 40Ω, which is marked as red arrow with (1) in Fig.15 (b). Then, the ASF-Beta method and the Search Mode are alternatively triggered as the trajectory (2) $\rightarrow \cdots \rightarrow$ (6). After (6), all of the β ranges have been scanned, and operating point goes back to the "region $n = 3$". From Fig.15(a), there are only 7 steps for the proposed technique to relocate the GMPP after the load changes. Furthermore, it also proves that the proposed technique can be well used for the load variation condition.

D. Evaluation

Finally, the comparison among these GMPPT techniques for different PSC patterns is summarized in TABLE II. In TABLE II, the term "Time" refers to the required tracking time for GMPP. For Pattern III, both of the technique in [3] with $\Delta P_{interval} = 20W$ and the technique in [4] can only track the LMPPs. Thus, the "Time" for these techniques refers to the required tracking time for LMPP.

The terms "Tracking" and "Steady-state" refer to the dynamic tracking efficiency and steady-state efficiency for these GMPPT techniques, respectively. For the dynamic tracking efficiency, it is express as

$$\eta_{dyn} = \frac{\sum_0^{T_M} P_{pv}}{P_{max} \cdot T_M} \tag{9}$$

where P_{pv}isthe measured values of the power, P_{max} is the theoretical maximum value of the power, and T_M is the total measurement time. For a fair comparison, T_M is set as the required longest tracking time among these GMPPT techniques [31], namely $0.57s$, $0.69s$ and $0.48s$ for Pattern I, Pattern II and Pattern III, respectively.

After T_M, the P&O method and INC method are used, and all of these GMPPT techniques work in their steady-state stage. Then, a three-level oscillation with a period of $4T_p$ is commonly happened [32, 33]. Therefore, the steady-state efficiency is expressed as

$$\eta_{stat} = \frac{\sum_{T_M}^{T_M+4\cdot T_p} P_{pv}}{P_{max} \cdot 4 \cdot T_p} \tag{10}$$

From TABLE II, it can be seen that the proposed technique requires the shortest time to track the GMPP with the overall highest tracking efficiency. Furthermore, it should be noted that the steady-state efficiency for the technique in [3] with $\Delta P_{interval} = 20W$ and the technique in [4] are the lowest for the Pattern III.

V. Experimental Results

In order to verify the effectiveness of the proposed algorithm, the experiments comparison among these GMPPT

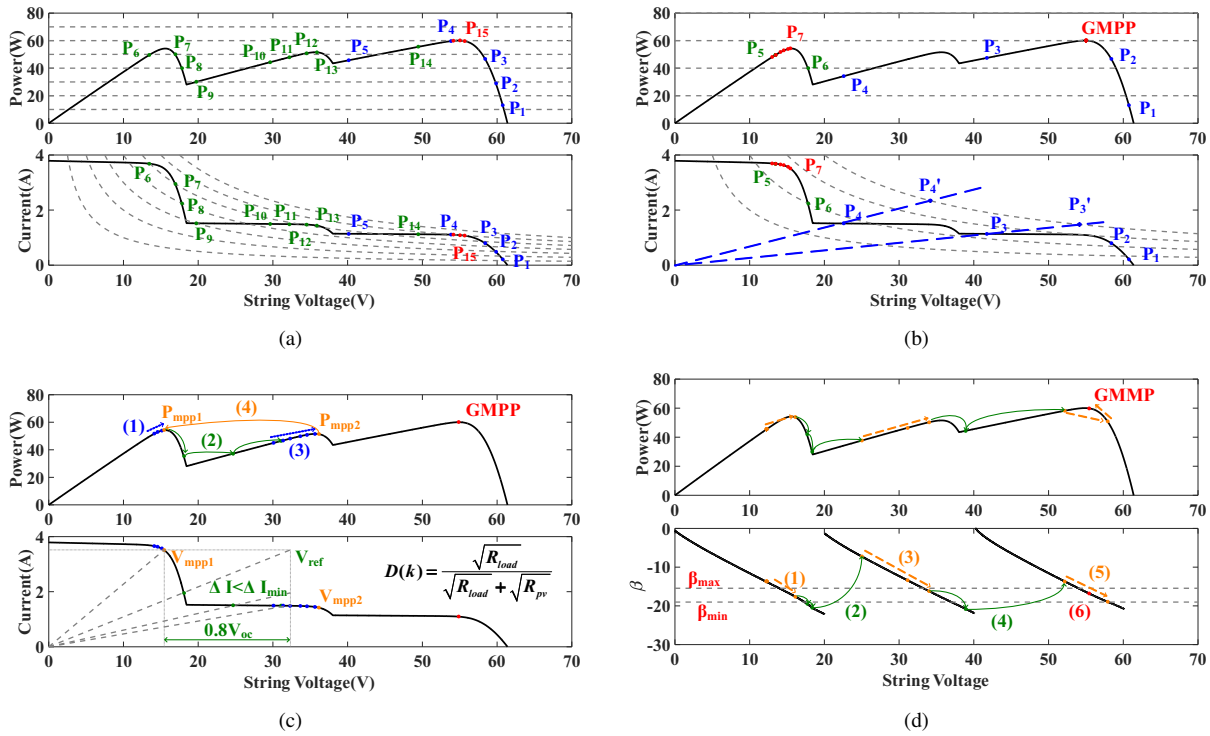

Fig. 14. Tracking details for Pattern III: (a) the technique in [3] with $\Delta P_{interval} = 10W$; (b) the technique in [3] with $\Delta P_{interval} = 20W$; (c) the technique in [4]; (d) the proposed technique.

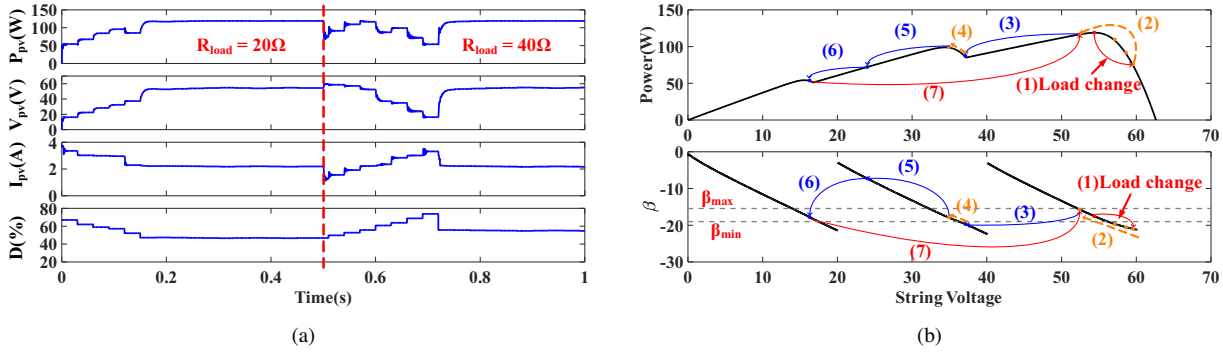

Fig. 15. Simulation results for load variation: (a) the overview performance of the proposed technique; (b) the tracking details.

techniques for different PSC patterns was performed on the same experimental prototype, as shown in Fig.16. Main specification of the main components is shown in TABLE III. The PV emulator Chroma ATE-62050H-600S, which is a programmable DC supply, was used to emulate solar module characteristics. The dSPACE DS1104 was adopted as a control platform and various MPPT algorithms were implemented. The electronic load, IT8514C+, was used for load variation analysis. Since the PV emulator has a limited dynamic speed, which is much slower than that of a practical crystalline PV module [34]. Therefore, the sampling time T_p for the MPPT controller in the experiments was set as $0.5s$.

Three two-stage GMPPT algorithms are evaluated, namely the technique in [3], the technique in [4], and the proposed technique. Same as the simulation, two different value of $\Delta P_{interval}$, $10W$ and $20W$, are used for the technique in [3]. The fixed step size is set as 0.5% for the technique in [3] and the technique in [4]. In the experimental evaluation of different GMPPT algorithms, three PSC patterns are used, which are also set the same as the simulation.

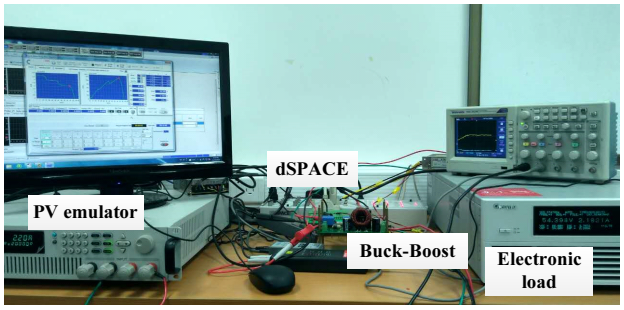

Fig. 16. Experimental test bench.

Fig.17 shows the experimental results for the Pattern I.

TABLE II
COMPARISON OF THE SIMULATION RESULTS FOR DIFFERENT PSC PATTERNS

Technique		Pattern I Time	Pattern I Tracking	Pattern II Time	Pattern II Tracking	Pattern III Time	Pattern III Tracking	Steady-state
Technique in [3]	10W	0.45s	72.87%	0.42s	79.35%	**0.48s**	77.94%	98.76%
	20W	0.24s	81.22%	0.30s	87.56%	0.39s	81.91%	90.58%
Technique in [4]		**0.57s**	75.98%	**0.69s**	77.45%	0.42s	80.58%	90.57%
Proposed technique		0.18s	90.05%	0.27s	89.75%	0.30s	85.77%	99.40%

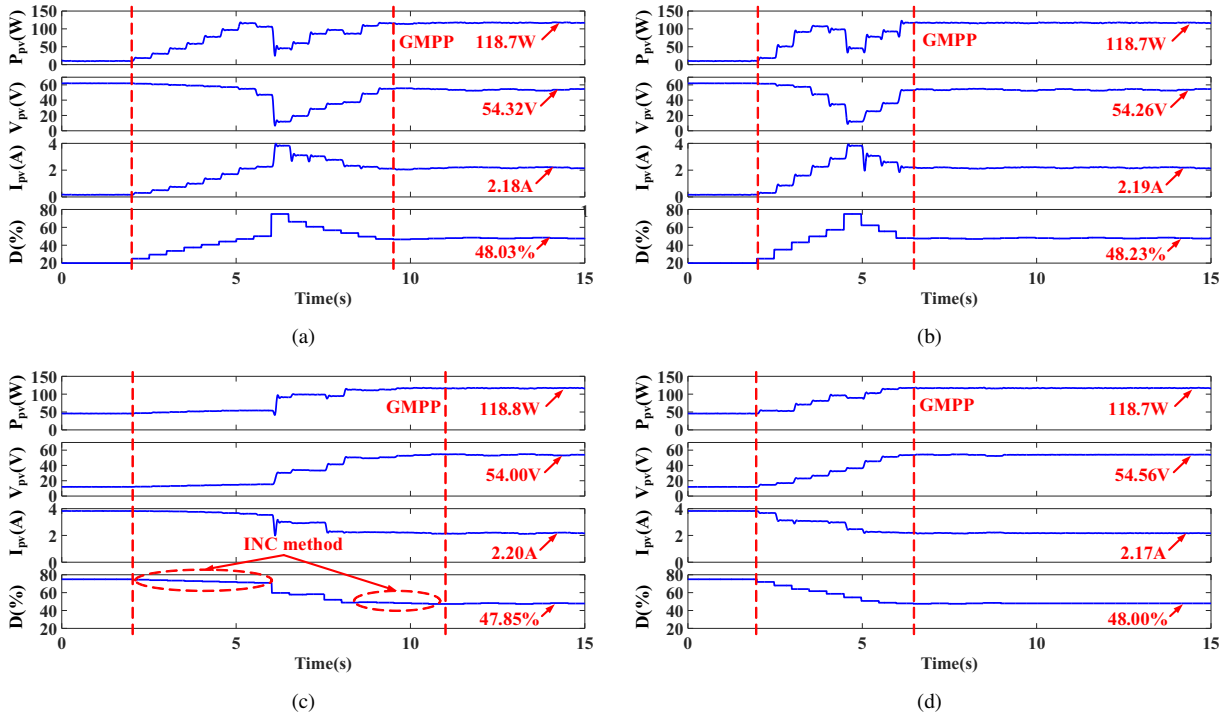

Fig. 17. Experimental results for the pattern I: (a) the technique in [3] with $\Delta P_{interval} = 10W$; (b) the technique in [3] with $\Delta P_{interval} = 20W$; (c) the technique in [4]; (d) the proposed technique.

TABLE III
MAIN COMPONENTS SPECIFICATION FOR THE PROTOTYPE

Parameter	Value
Electrolytic capacitor C_{in}	$470uF$
Electrolytic capacitor C_{out}	$100uF$
Inductor L	$1mH$
IGBT	IRG4PH50U
Diode	RHRG30120
Current transducer	LA25-NP
Voltage transducer	LV25-P
Switching frequency	$20kHz$

The technique in [3] initially starts from the vicinity of the string open-circuit voltage and the duty cycle for the buck-boost converter is regulated at 20%. At time $t = 2s$, the technique in [3] starts to scan the rest of the P–V curve by $\Delta P_{interval}$. With $\Delta P_{interval} = 10W$, the technique in [3] needs $7.5s$ (15 steps) to reach the vicinity of the GMPP. With $\Delta P_{interval} = 20W$, the vicinity of the GMPP can be initially tracked by the technique in [3] within $4.5s$ (9 steps), as illustrated by Fig.17(b).

The technique in [4] starts at time $t = 2s$, where the duty cycle for the buck-boost converter is regulated as 75%, as shown in Fig.17(c). Then, the INC method is used to find the first MPP. After that, a large voltage increment by $0.8V_{oc}$ is used to skips to the vicinity of the second MPP. This process is repeated until the power at the next MPP is smaller than the previous one, or the OP reaches the rightmost of the P–V curve. Since each MPP must be determined by the INC method, this technique requires the longest time to locate the GMPP, which is $9ss$ (18 steps).

Same to the technique in [4], the proposed technique also starts at time $t = 2s$, where the duty cycle for the buck-boost converter is set as 75%, as shown in Fig.17(d). However, compared to the technique in [4], the proposed technique can quickly locate the vicinities of the each MPP rather than the exact locations. Thus, the proposed technique only requires $4.5s$ (9 steps) to locate the GMPP. Furthermore, it should be noted that the proposed technique shows zero oscillation at the steady state.

For the Pattern II, the technique in [3] with $\Delta P_{interval} = 20W$ requires the shortest time, namely $4.5s$ (9 steps), to

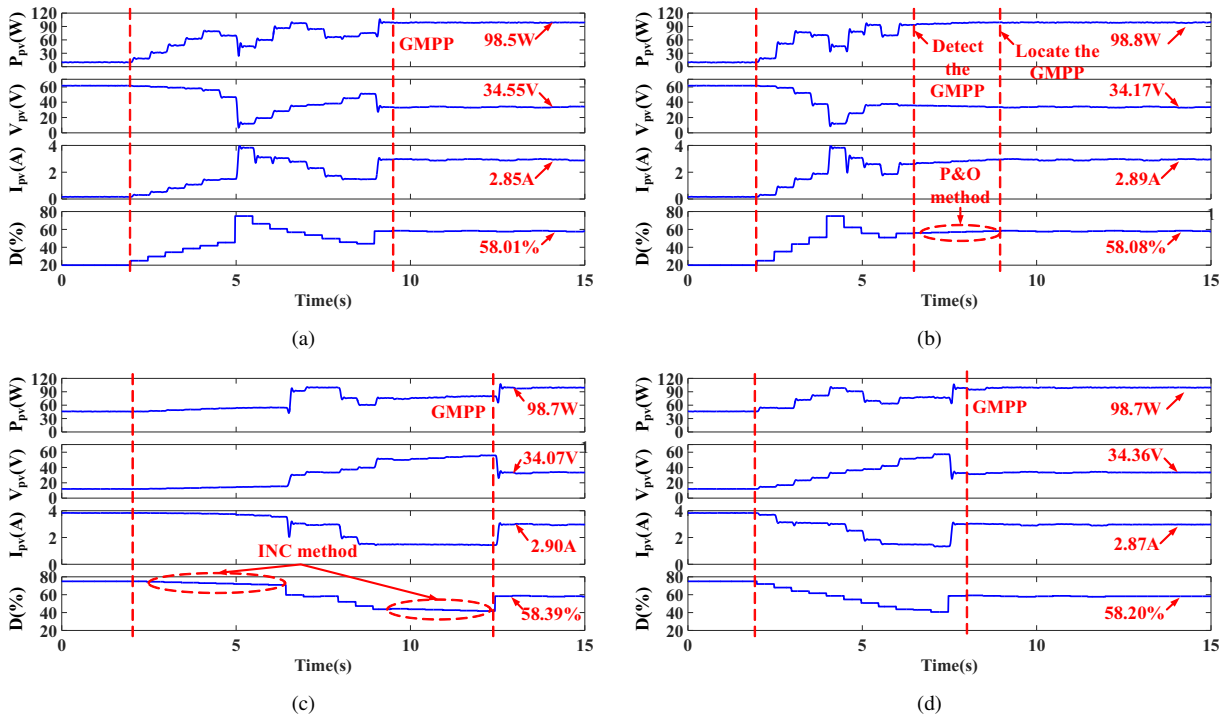

Fig. 18. Experimental results for the pattern II: (a) the technique in [3] with $\Delta P_{interval} = 10W$; (b) the technique in [3] with $\Delta P_{interval} = 20W$; (c) the technique in [4]; (d) the proposed technique.

detect the vicinity of the GMPP. However, it needs $2.5s$ (5 steps) to locate the real GMPP by P&O method. Therefore, the total tracking time of this technique is $7s$ (14 steps), which is slightly longer than the proposed technique, $6s$ (12 steps). Following the proposed technique, the technique in [3] with $\Delta P_{interval} = 10W$ requires $7.5s$ (15 steps). The technique in [4] also requires the longest time to locate the GMPP, which is $11s$ (22 steps).

For the Pattern III, the technique in [3] with $\Delta P_{interval} = 20W$ and the technique in [4] cannot correctly track the GMPP, which is the same as the simulation results. As shown in Fig.19 (b) and (c), only the LMPP is located. The technique in [3] with $\Delta P_{interval} = 10W$ requires the shortest time, namely $3.5s$ (7 steps), to detect the vicinity of the GMPP. However, it needs $5.5s$ (11 steps) to locate the real GMPP by P&O method. Therefore, the overall tracking time for the proposed technique is still the shortest, $5.5s$ (11 steps), compared to $9s$ (18 steps) for the technique in [3] with $\Delta P_{interval} = 10W$.

Finally, the experimental results are summarised in TABLE IV. The terms defined in TABLE IV is exactly same as that in TABLE II. Furthermore, the dynamic tracking efficiency and steady-state efficiency are calculated by (9) and (10). It should be noted that T_M for Pattern I, Pattern II and Pattern III are set as $9.0s$, $11.0s$, $9.0s$, respectively.

VI. Conclusion

The main contribution of this paper is the proposed novel two-stage GMPPT method for GMPPT tracking and partial shading detection in PV systems by modifying the conventional Beta method. Firstly the PV string equivalent model has been built up, thus, the I-V curve with multiple peaks can be equivalent represented as several I-V curves with single peak, which significantly simplify the GMPPT tracking for PV strings under various partial shading conditions. Following this mathematical model, some advanced MPPT algorithm for conventional PV systems under normal condition can be applied for complicated partial shading conditions. Motivated by the advantages of the Beta method, such as fast tracking speed, zero oscillations for steady state, and simple implementation, this paper aims to propose and verify a novel beta parameter based GMPPT algorithm for complicated PSC application. In this paper, different PSC patterns were discussed and the modified beta algorithm was discussed with mathematical expressions, implementation flowcharts and detailed tracking process analysis. Both simulation and experimental comparison of the proposed algorithm with other widely discussed algorithms was conducted for different PSC patterns. Since the proposed algorithm searches the vicinity of the parameter β rather than $0.8V_{oc}$, it shows significant advantages compared with other techniques:

(1) It can track the GMPPT under any PSC patterns;
(2) It inherently detect the PSC occurrence without setting any threshold parameters or periodical interruption, which reduce the implementation difficulty;
(3) It is more accurate than the previous techniques;
(4) The tracking speed of the proposed technique is fastest among these discussed algorithms;
(5) It achieves the zero oscillations for the steady state.

VII. Acknowledgement

This work was supported by the Research development fund of XJTLU (RDF-14-02-03), the Jiangsu Science and Technol-

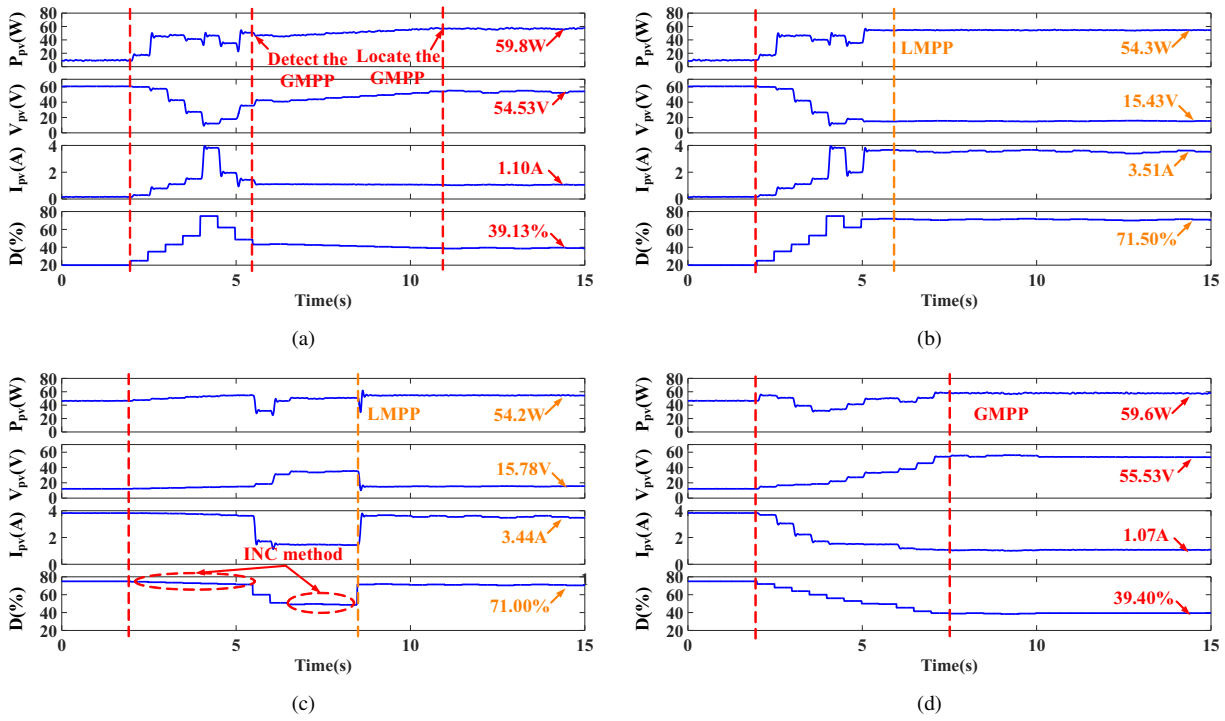

Fig. 19. Experimental results for the pattern III: (a) the technique in [3] with $\Delta P_{interval} = 10W$; (b) the technique in [3] with $\Delta P_{interval} = 20W$; (c) the technique in [4]; (d) the proposed technique.

TABLE IV
COMPARISON OF THE EXPERIMENTAL RESULTS FOR DIFFERENT PSC PATTERNS

Technique		Pattern I Time	Pattern I Tracking	Pattern II Time	Pattern II Tracking	Pattern III Time	Pattern III Tracking	Steady-state
Technique in [3]	10W	7.5s	72.70%	7.0s	76.30%	9.0s	83.83%	98.05%
	20W	4.5s	82.04%	7.5s	85.23%	6.0s	86.84%	90.14%
Technique in [4]		9.0s	69.37%	11.0s	69.54%	7.0s	89.19%	90.18%
Proposed technique		4.5s	86.47%	6.0s	86.60%	5.5s	90.13%	99.12%

ogy Programme (BK20161252), the Visiting Scholarship of State Key Laboratory of Power Transmission Equipment & System Security and New Technology (2007DA10512716414), and the National Nature Science Foundation of China (51407145).

X. Li and H. Wen are with the Xian Jiaotong-Liverpool University, Suzhou 215123, China (e-mail: Xingshuo.Li@xjtlu.edu.cn; Huiqing.Wen@xjtlu.edu.cn).

Y. Hu and L. Jiang are with the University of Liverpool, Liverpool, L69 3BX, U.K.(e-mail: Y.Hu35@liverpool.ac.uk; L.Jiang@liverpool.ac.uk).

W. Xiao is with the University of Sydney, Sydney, NSW 2006, Australia. (e-mail: weidong.xiao@sydney.edu.au).

REFERENCES

[1] B. Subudhi and R. Pradhan, "A comparative study on maximum power point tracking techniques for photovoltaic power systems," *IEEE Trans. Sustain. Energy*, vol. 4, no. 1, pp. 89–98, Jan. 2013.

[2] M. de Brito, L. Galotto, L. Sampaio, G. de Azevedo e Melo, and C. Canesin, "Evaluation of the main mppt techniques for photovoltaic applications," *IEEE Trans. Ind. Electron*, vol. 60, no. 3, pp. 1156–1167, Mar. 2013.

[3] E. Koutroulis and F. Blaabjerg, "A new technique for tracking the global maximum power point of pv arrays operating under partial-shading conditions," *IEEE J. Photovoltaics*, vol. 2, no. 2, pp. 184–190, Apr. 2012.

[4] K. S. Tey and S. Mekhilef, "Modified incremental conductance algorithm for photovoltaic system under partial shading conditions and load variation," *IEEE Trans. Ind. Electron*, vol. 61, no. 10, pp. 5384–5392, Oct. 2014.

[5] A. Bidram, A. Davoudi, and R. S. Balog, "Control and circuit techniques to mitigate partial shading effects in photovoltaic arrays," *IEEE J. Photovoltaics*, vol. 2, no. 4, pp. 532–546, Oct. 2012.

[6] Y.-H. Liu, J.-H. Chen, and J.-W. Huang, "A review of maximum power point tracking techniques for use in partially shaded conditions," *Renew. Sust. Energ. Rev.*, vol. 41, pp. 436–453, 2015.

[7] B. N. Alajmi, K. H. Ahmed, S. J. Finney, and B. W. Williams, "A maximum power point tracking technique for partially shaded photovoltaic systems in microgrids," *IEEE Trans. Ind. Electron*, vol. 60, no. 4, pp. 1596–1606, Apr. 2013.

[8] K. Ishaque, Z. Salam, M. Amjad, and S. Mekhilef, "An improved particle swarm optimization (pso) based mppt for pv with reduced steady-state oscillation," *IEEE Trans. Power Electron.*, vol. 27, no. 8, pp. 3627–3638, Aug. 2012.

[9] K. Ishaque and Z. Salam, "A deterministic particle swarm opti-

mization maximum power point tracker for photovoltaic system under partial shading condition," *IEEE Trans. Ind. Electron*, vol. 60, no. 8, pp. 3195–3206, Aug. 2013.
[10] K. Sundareswaran, S. Peddapati, and S. Palani, "Mppt of pv systems under partial shaded conditions through a colony of flashing fireflies," *IEEE Trans. Energy Convers.*, vol. 29, no. 2, pp. 463–472, Jun. 2014.
[11] K. Sundareswaran, P. Sankar, P. S. R. Nayak, S. P. Simon, and S. Palani, "Enhanced energy output from a pv system under partial shaded conditions through artificial bee colony," *IEEE Trans. Sustain. Energy*, vol. 6, no. 1, pp. 198–209, Jan. 2015.
[12] K. Sundareswaran, V. Vigneshkumar, P. Sankar, S. P. Simon, P. S. R. Nayak, and S. Palani, "Development of an improved p&o algorithm assisted through a colony of foraging ants for mppt in pv system," *IEEE Trans. Ind. Informat.*, vol. 12, no. 1, pp. 187–200, Feb. 2016.
[13] S. Mohanty, B. Subudhi, and P. K. Ray, "A new mppt design using grey wolf optimization technique for photovoltaic system under partial shading conditions," *IEEE Trans. Sustain. Energy*, vol. 7, no. 1, pp. 181–188, Jan. 2016.
[14] S. Lyden and M. E. Haque, "A simulated annealing global maximum power point tracking approach for pv modules under partial shading conditions," *IEEE Trans. Power Electron.*, vol. 31, no. 6, pp. 4171–4181, Jun. 2016.
[15] T. L. Nguyen and K. S. Low, "A global maximum power point tracking scheme employing direct search algorithm for photovoltaic systems," *IEEE Trans. Ind. Electron*, vol. 57, no. 10, pp. 3456–3467, Oct. 2010.
[16] N. A. Ahmed and M. Miyatake, "A novel maximum power point tracking for photovoltaic applications under partially shaded insolation conditions," *Electr. Pow. Syst. Res.*, vol. 78, no. 5, pp. 777–784, 2008.
[17] Q. Zhang, C. Hu, L. Chen, A. Amirahmadi, N. Kutkut, Z. J. Shen, and I. Batarseh, "A center point iteration mppt method with application on the frequency-modulated llc microinverter," *IEEE Trans. Power Electron.*, vol. 29, no. 3, pp. 1262–1274, Mar. 2014.
[18] G. Carannante, C. Fraddanno, M. Pagano, and L. Piegari, "Experimental performance of mppt algorithm for photovoltaic sources subject to inhomogeneous insolation," *IEEE Trans. Ind. Electron*, vol. 56, no. 11, pp. 4374–4380, Nov. 2009.
[19] Y. H. Ji, D. Y. Jung, J. G. Kim, J. H. Kim, T. W. Lee, and C. Y. Won, "A real maximum power point tracking method for mismatching compensation in pv array under partially shaded conditions," *IEEE Trans. Power Electron.*, vol. 26, no. 4, pp. 1001–1009, Apr. 2011.
[20] H. Patel and V. Agarwal, "Maximum power point tracking scheme for pv systems operating under partially shaded conditions," *IEEE Trans. Ind. Electron*, vol. 55, no. 4, pp. 1689–1698, Apr. 2008.
[21] K. Chen, S. Tian, Y. Cheng, and L. Bai, "An improved mppt controller for photovoltaic system under partial shading condition," *IEEE Trans. Sustain. Energy*, vol. 5, no. 3, pp. 978–985, Jul. 2014.
[22] Y. Wang, Y. Li, and X. Ruan, "High-accuracy and fast-speed mppt methods for pv string under partially shaded conditions," *IEEE Trans. Ind. Electron*, vol. 63, no. 1, pp. 235–245, Jan. 2016.
[23] J. Ahmed and Z. Salam, "An improved method to predict the position of maximum power point during partial shading for pv arrays," *IEEE Trans. Ind. Informat.*, vol. 11, no. 6, pp. 1378–1387, Dec. 2015.
[24] S. Jain and V. Agarwal, "A new algorithm for rapid tracking of approximate maximum power point in photovoltaic systems," *IEEE Power Electron. Lett.*, vol. 2, no. 1, pp. 16–19, Mar. 2004.
[25] ——, "Comparison of the performance of maximum power point tracking schemes applied to single-stage grid-connected photovoltaic systems," *IET Electr. Power Appl.*, vol. 1, no. 5, pp. 753–762, Sep. 2007.
[26] X. Li, H. Wen, and C. Zhao, "Improved beta parameter based mppt method in photovoltaic system," in *Proc. IEEE 9th Int. Power Electron. ECCE Asia Conf.*, Jun. 2015, pp. 1405–1412.
[27] E. I. Batzelis, G. E. Kampitsis, S. A. Papathanassiou, and S. N. Manias, "Direct mpp calculation in terms of the single-diode pv model parameters," *IEEE Trans. Energy Convers.*, vol. 30, no. 1, pp. 226–236, Mar. 2015.
[28] E. I. Batzelis, I. A. Routsolias, and S. A. Papathanassiou, "An explicit pv string model based on the lambert w function and simplified mpp expressions for operation under partial shading," *IEEE Trans. Sustain. Energy*, vol. 5, no. 1, pp. 301–312, Jan. 2014.
[29] X. Li, H. Wen, L. Jiang, Y. Hu, and C. Zhao, "An improved beta method with auto-scaling factor for photovoltaic system," *IEEE Trans. Ind. Appl.*, vol. 52, no. 5, pp. 4281–4291, Sep. 2016.
[30] X. Li, H. Wen, L. Jiang, W. Xiao, Y. Du, and C. Zhao, "An improved mppt method for pv system with fast-converging speed and zero oscillation," *IEEE Trans. Ind. Appl.*, vol. 52, no. 6, pp. 5051–5064, Nov. 2016.
[31] H. Yohan, S. N. Pham, Y. Taegeun, C. Kookbyung, B. Kwang-Hyun, and K. Yong Sin, "Efficient maximum power point tracking for a distributed pv system under rapidly changing environmental conditions," *IEEE Trans. Power Electron.*, vol. 30, no. 8, pp. 4209–4218, Aug. 2015.
[32] N. Femia, G. Petrone, G. Spagnuolo, and M. Vitelli, "Optimization of perturb and observe maximum power point tracking method," *IEEE Trans. Power Electron.*, vol. 20, no. 4, pp. 963–973, Jul. 2005.
[33] F. Paz and M. Ordonez, "Zero oscillation and irradiance slope tracking for photovoltaic mppt," *IEEE Trans. Ind. Electron*, vol. 61, no. 11, pp. 6138–6147, Nov. 2014.
[34] W. Xiao, H. H. Zeineldin, and Z. Peng, "Statistic and parallel testing procedure for evaluating maximum power point tracking algorithms of photovoltaic power systems," *IEEE J. Photovoltaics*, vol. 3, no. 3, pp. 1062–1069, Jul. 2013.

Xingshuo Li was born in Zhengzhou, China. He received his B.S. in Computer Science from Zhengzhou University, Zhengzhou, China, in 2012, and M.S. in Sustainable Energy Technology with distinction from Xi'an Jiaotong-Liverpool University. He is currently working towards the Ph.D. degree at University of Liverpool, U.K. His research interests include digital control, power electronics, and power converters for Photovoltaic.

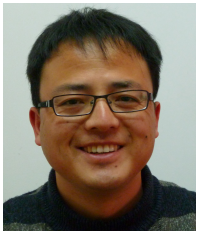

Huiqing Wen (M'13) received his B.S. and M.S. degrees in Electrical Engineering from Zhejiang University, Hangzhou, China, in 2002 and 2006, respectively. In 2009, he received his Ph.D. in Electrical Engineering from the Chinese Academy of Sciences, Beijing, China. From 2009 to 2010, he has been an electrical engineer working with the GE (China) Research and Development Center Company, Ltd., Shanghai, China. From 2010 to 2011, he was an engineer at the China Coal Research Institute, Beijing, China. From 2011 to 2012, he was a postdoctoral fellow at the Masdar Institute of Science and Technology, Abu Dhabi, United Arab Emirates. In 2013, he joined the Electrical and Electronic Engineering Department of Xi'an Jiaotong-Liverpool University (XJTLU), Suzhou, China. Currently, he is an associate professor at the XJTLU. His research interests include bidirectional DC-DC converter, power electronics in flexible AC transmission applications, electrical vehicles, and high-power, three-level electrical driving systems.

Yihua Hu (M'13-SM'15) received the B.S. degree in electrical motor drives in 2003, and the Ph.D. degree in power electronics and drives in 2011, both from China University of Mining and Technology, Jiangsu, China. Between 2011 and 2013, he was with the College of Electrical Engineering, Zhejiang University as a Postdoctoral Fellow. Between November 2012 and February 2013, he was an academic visiting scholar with the School of Electrical and Electronic Engineering, Newcastle University, Newcastle upon Tyne, UK. Between 2013 and 2015, he worked as a Research Associate at the power electronics and motor drive group, the University of Strathclyde. Currently, he is a Lecturer at the Department of Electrical Engineering and Electronics, University of Liverpool (UoL). He has published more than 60 peer reviewed technical papers in leading journals. His research interests include PV generation system, power electronics converters control, and electrical motor drives. He is the associate editor of IET Power Electronics, IET Renewable Power Generation, and Journal of Power Electronics.

Lin Jiang received his B.S. and M.E. degrees from Huazhong University of Science and Technology, China, and his Ph.D. from the University of Liverpool, Liverpool, U.K., all in Electrical Engineering, in 1992, 1996, and 2001, respectively. He is a readerr of Electrical Engineering at the University of Liverpool. His research interests include optimization and control of smart grid/electrical machine/power electronics and renewable energy.

Weidong Xiao (SM13) received the Masters and the Ph.D. degrees in electrical engineering from the University of British Columbia, Vancouver, Canada, in 2003 and 2007 respectively. Dr. Xiao is an Associate Professor with the school of Electrical and Information Engineering, University of Sydney, Australia. From 2010 to 2016, he has been working with Masdar Institute of Science and Technology, Abu Dhabi, United Arab Emirates. In 2010, he was a Visiting Scholar with the Massachusetts Institute of Technology (MIT), Cambridge, USA, where he worked on the power interfaces for PV power systems. Prior to the academic career, he worked as a R&D engineering manager with MSR Innovations Inc., Burnaby, Canada, focusing on integration, research, optimization and design of photovoltaic power systems. His research interest includes photovoltaic power systems, power electronics, dynamic systems and control, and industry applications. Dr. Xiao is presently an Associate Editor of the IEEE Transactions on Industrial Electronics.